

Improving Action Smoothness of a Cascaded Online Learning Flight Control System

Yifei Li, Erik-Jan van Kampen

Abstract

The online reinforcement learning flight control has demonstrated the ability of adaptively adjusting the control policy by policy gradient without explicitly requiring the dynamical model. Although the cascaded structure of the controller has shown the advantage of enabling efficient policy learning in angle-of-attack tracking control with the control surface deflection, its tracking error and stability can be degraded by oscillatory control actions. To address this issue, we incorporate temporal policy regularization and a low-pass second-order filter techniques into the cascaded flight control framework, to reduce both the amplitude and oscillatory frequency of the control actions. The Fast Fourier Transform (FFT) is employed to analyze action smoothness in the frequency domain. Flight control simulations demonstrate the effectiveness of the two proposed techniques.

Index Terms

reinforcement learning, symmetry, data augmentation, approximate value iteration, flight control.

I. INTRODUCTION

Online reinforcement learning (RL) has been applied to flight control design to achieve data-driven optimization of control policies. The gradients of a control policy is constructed using measured state samples. This approach saves significant efforts for control design in modeling a complex nonlinear system, enabling *model-free* control design. In contrast, model-based designs of optimal control, such as Model Predictive Control (MPC), Linear Quadratic Regulator (LQR) and Approximate Dynamic Programming (ADP), use a system model to predict future states and then optimize the control policy at current states, a process referred to as programming. The system model has significant influences on control performance, including optimality and stability. Consequently, applying these methods to complex nonlinear systems, such as aircraft, is challenging because accurate models are not always available.

The implementation of online reinforcement learning using ADP does not necessarily learn a fully networked model, since only the first-order derivatives of system dynamics are needed to construct policy gradients. This fact motivates utilizing a simple model with fewer parameters, but captures the first-order derivatives, such as incremental model. The incremental model is a local linear model of a nonlinear system, derived using the Taylor expansion method. The combination of incremental model and linear Recursive Least Square (RLS) identification leads to the development of innovative incremental model-based ADP (IADP) methods, achieving computation-efficient online policy learning. Flight control applications are seen for angle-of-attack (AOA) tracking, pitch rate tracking and altitude tracking systems. The variants of IADP include incremental model-based heuristic dynamic Programming (IHDP), incremental model-based dual heuristic programming (IDHP) and incremental model-based global dual heuristic programming (IGDHP).

A cascaded structure of the flight controller is usually used in AOA tracking control systems, enabling separate control of angle of attack tracking in the outer loop and pitch rate tracking in the inner loop. This hierarchical control strategy integrates explicit pitch rate constraints and thereby reduces action oscillations. Although the pitch rate can be constrained through a penalization mechanism when training an integrated control structure, this approach does not explicitly learn a pitch rate reference policy, degrading the control performance. The importance of a well-designed pitch rate reference in ensuring better control performance has been demonstrated in backstepping method, where a stabilizing pitch rate reference policy is derived by employing a nominal system model.

However, designing a stabilizing pitch rate reference is impossible in the ADP framework, given the unavailability of a system model. The initial pitch rate reference is randomly settled so that the process of policy learning may lose smooth pitch rate control, leading to state oscillations or even instability. Moreover, the time-varying nonlinear dynamics pose additional challenges on the control performance. As a result, the pitch rate reference exhibits switching behaviors in response to tracking errors, which further disturbs the control surface deflection in the inner loop (a phenomenon also observed in backstepping control).

The second reason accounting for state oscillations in IADP is the saturation of the actor. As the activation functions become saturated during the weight updates, the actor exhibits an equivalent bang–bang control behavior. The saturated activation

Yifei Li was with the Section Control and Simulation, Faculty of Aerospace Engineering, Delft University of Technology, Delft, 2629 HS, the Netherlands, e-mail: y.li-34@tudelft.nl.

Erik-Jan van Kampen was with the Section Control and Simulation, Faculty of Aerospace Engineering, Delft University of Technology, Delft, 2629 HS, the Netherlands, e-mail: e.vankampen@tudelft.nl.

Manuscript received Month Day, Year; revised Month Day, Year.

functions also produce vanishing policy gradients, making the actor weights nearly fixed and difficult to adjust. This issue can be eased by using a discounted learning rate that slows down the actor update as the learning proceeds. The actor weights are then less likely to enter the saturation region of the activation function. However, the selection of a learning rate is empirical and is sensitive to the performance of delaying saturation. More importantly, this approach does not fully prevent saturation as learning proceeds over time. The second solution is to terminate actor learning at a certain time by fixing its weights. This also requires careful design of the termination timing or other termination conditions.

This paper addresses the state oscillation by introducing a temporal smoothness loss into the online policy optimization. This has been applied in offline reinforcement learning but not in online learning settings. Based on the results in this paper, showing that this method does not suppress high-frequency actions, we introduce the low-pass filter to further smoothen the actions, which demonstrates effective filtering in command-filter backstepping.

The main contributions of this work are summarized as follows:

- The temporal smoothness technique is introduced for online policy regularization, formulated as a multi-objective optimization framework.
- A low-pass filter is incorporated to smooth the pitch-rate reference, improving the action smoothness.

The remainder of this paper is structured as follows. Section II presents the aerial vehicle dynamics and a discrete-time model. Section III presents optimization-based control design for angle-of-attack tracking. Section IV presents the online learning framework, followed by the introductions of two action smoothness techniques in Section V. Section VI presents comparative simulations of control systems with action smoothness techniques. Section VII concludes this paper.

II. MODEL

A. Aerial Vehicle Model

The dynamical model of aerial vehicles is given as [32]

$$\begin{aligned}\dot{\alpha} &= \left(\frac{fgQS}{WV} \right) \cos(\alpha) [\phi_z(\alpha) + b_z \delta] + q \\ \dot{q} &= \left(\frac{fQScd}{I_{yy}} \right) [\phi_m(\alpha) + b_m \delta]\end{aligned}\tag{1}$$

where α, q are angle-of-attack, pitch rate, δ is the control surface deflection. The aerodynamic coefficients are approximately computed by $b_z = -0.034, b_m = -0.206$, and

$$\begin{aligned}\phi_z(\alpha) &= 0.000103\alpha^3 - 0.00945\alpha|\alpha| - 0.170\alpha \\ \phi_m(\alpha) &= 0.000215\alpha^3 - 0.0195\alpha|\alpha| - 0.051\alpha\end{aligned}\tag{2}$$

These approximations of $b_z, b_m, \phi_z(\alpha), \phi_m(\alpha)$ hold for α in the range of ± 20 degrees. The physical coefficients are provided in Table I. In addition, the actuator dynamics are considered as a first order model with the time constant $0.005s$. The rate limit is 600 deg/s , and a control surface deflection limit is ± 20 degrees.

TABLE I: Physical parameters (adapted from [32])

Notations	Definition	Value
g	acceleration of gravity	9.815 m/s ²
W	weight	204.3 kg
V	speed	947.715 m/s
I_{yy}	pitch moment of inertia	247.438 kg·m ²
f	radians to degrees	180/π
Q	dynamic pressure	29969.861 kg/m ²
S	reference area	0.041 m ²
d	reference diameter	0.229 m

B. Strict-feedback Single-Input-Single-Output System

The differential equations 1 can be reformulated as

$$\begin{aligned}\dot{x}_1 &= f_1(x_1) + x_2 + d_1(x_1, u) \\ \dot{x}_2 &= f_2(x_1) + g_2 u\end{aligned}\tag{3}$$

where $[x_1, x_2]^T = [\alpha, q]^T$, $u = \delta$ are state and control input. The nonlinear functions are defined as

$$\begin{aligned} f_1(x_1) &= \left(\frac{fgQS}{WV} \right) \cos(\alpha) \phi_z(\alpha), & d_1(x_1, u) &= \left(\frac{fgQS}{WV} \right) \cos(\alpha) b_z \\ f_2(x_1) &= \left(\frac{fQSD}{I_{yy}} \right) \phi_m(\alpha), & g_2(x_1, \delta) &= \left(\frac{fQSD}{I_{yy}} \right) b_m \end{aligned} \quad (4)$$

The single-input-single-output (SISO) system has a single input controlling the second state x_2 and subsequently controls the first state x_1 through a integrator dynamics, which shows dynamical oscillations in the control process. Simple examples are inverted pendulum, Van der Pol oscillator. However, the angle-of-attack dynamics also have internal dynamics f_1 , making rate control challenging. This motivates the separate control designs for angle-of-attack and pitch rate.

III. OPTIMIZATION-BASED CONTROL DESIGN

This section firstly derives the tracking error dynamics. The optimization-based tracking control approach is then formulated to achieve optimal tracking control of angle-of-attack and pitch rate.

A. Tracking errors dynamics

Define the tracking errors as $e_1 = \alpha - \alpha_{\text{ref}}$, $e_2 = q - q_{\text{ref}}$, one has

$$\begin{aligned} \dot{e}_1 &= \dot{\alpha} - \dot{\alpha}_{\text{ref}} \\ &= f_1(x_1) + x_2 + d_1 - \dot{\alpha}_{\text{ref}} \\ &= f_1(x_1) + e_2 + q_{\text{ref}} + d_1 - \dot{\alpha}_{\text{ref}} \end{aligned} \quad (5)$$

$$\begin{aligned} \dot{e}_2 &= \dot{q} - \dot{q}_{\text{ref}} \\ &= f_2(x_1) + g_2 u - \dot{q}_{\text{ref}} \end{aligned} \quad (6)$$

where α_{ref} , q_{ref} are the angle-of-attack reference and the pitch rate reference.

The virtual control defined as $q_{\text{ref}} = v(e_\alpha, \alpha)$ is associated with e_α, α , aiming to provide error-feedback control for stabilizing e_α and compensate for the system dynamics associated with α_t . Its design has been studied in backstepping approaches using the knowledge of $f_1(x_1), d_1, \dot{x}_{1\text{ref}}$. The model uncertainties are dealt with adaptive laws to ensure asymptotic convergent of the tracking errors. However, this asymptotic convergence highly relies on the model knowledge and is degraded when the model is inaccurate. In model-free RL settings, the analytical design of $v(e_\alpha, \alpha)$ is infeasible when the dynamics f_1, d_1 are unknown. The policy is parameterized using a neural network and trained with samples. This situation also applies for the design of u in e_2 -subsystem.

B. Optimization-based tracking control

Infinite-horizon optimal tracking control problems are formulated to achieve angle-of-attack tracking and pitch rate tracking. The control laws are designed to minimize state-state-value functions associated with tracking errors and control efforts.

For the e_1 -subsystem, a state-value function starting from t is denoted as $V_1(t) : \mathbb{R}^2 \rightarrow \mathbb{R}_+$ and defined by

$$V_1(t) = \int_t^\infty c_1(t) dt \quad (7)$$

where $c_1(t) = e_1^2(t) + a q_{\text{ref}}^2(t)$ is the one-step cost of taking action $q_{\text{ref}}(t)$ at $e_1(t)$. $a > 0$ is a parameter that trades off between tracking error and control effort. \mathbb{R}_+ denotes the set of non-negative real numbers. Then the optimal control is defined as

$$q_{\text{ref}}^*(e_\alpha, \alpha, \delta) \in \arg \min_{q_{\text{ref}}} V_1(t) \quad (8)$$

The pitch rate reference is set as a function of e_1, α and δ in order to stabilize e_1 and compensate for the dynamics associated with α, δ . It serves as the input for the second tracking subsystem.

For the e_2 -subsystem, a state-value function starting from t is denoted as $V_2(t) : \mathbb{R}^2 \rightarrow \mathbb{R}_+$ and defined by

$$V_2(t) = \int_t^\infty c_2(t) dt \quad (9)$$

where $c_2(t) = e_2^2(t) + b u^2(t)$ is the one-step cost of taking action $u(t)$ at $e_2(t)$. $b > 0$ is a parameter that trades off between tracking error and control effort. Then the optimal control law is defined as

$$u^*(e_q, q, \alpha) \in \arg \min_u V_2(t) \quad (10)$$

Remark 1. The control surface deflection is designed as a function of e_2 , q and α , i.e., $\delta = u(e_2, q, \alpha)$, in order to stabilize e_2 and compensate for the dynamics associated with q, α .

IV. ONLINE REINFORCEMENT LEARNING IMPLEMENTATION

This section introduces an online reinforcement learning framework for angle-of-attack tracking control. A cascaded control structure is introduced for separate control of angle-of-attack tracking and pitch rate tracking [20], [22]. The learning process is a sample-based implementation of the optimization-based control design in Section III. The learning algorithm uses Incremental model-based heuristic dynamic programming (IHDP).

A. Incremental heuristic dynamic programming

IHDP can be employed to perform online model-free policy training [24]. The algorithm structure is shown in [24], [25]. The control-effectiveness matrix defined in the incremental model is used to construct the partial policy gradient from the next-step state to the action. Its linear characteristics provide a simple representation of the first derivatives of the system dynamics, thereby reducing the computational load during model training compared with a neural-network-based model in HDP. This advantage becomes more pronounced in model-free implementations of HDP and IHDP, where the model does not need to be accurate to ensure reliable state prediction and subsequent policy learning.

The incremental model is a local linear approximation of a nonlinear system. The incremental models of system are developed as

$$\begin{aligned} \Delta \hat{\alpha}_{t+1} &= F_{t-1}^1 \Delta \alpha_t + G_{t-1}^1 \Delta q_t \\ \Delta \hat{q}_{t+1} &= F_{t-1}^2 \Delta q_t + G_{t-1}^2 \Delta \delta_t \end{aligned} \quad (11)$$

where the subscript t denotes the discrete-time index.

The derivation is seen in Appendix VII-A.

B. Cascaded and networked control law

The cascaded control structure contains the outer-loop and the inner-loop actors, generating pitch rate reference and control surface deflection, respectively (see Figure 4). The training is based on the approximated value functions $\hat{V}_1(t)$, $\hat{V}_2(t)$. To implement model-free learning, the critic and actor networks are initialized randomly without incorporating any prior knowledge. The cascaded control structure is also seen in backstepping methods [12], [13], [14], [27].

Outer-loop control law

$$q_{\text{ref}}(e_1, \alpha, \delta) = W_2(e_1, \alpha, \delta) \quad (12)$$

Inner-loop control law

$$\delta(e_2, q, \alpha) = W_1(e_2, q, \alpha) \quad (13)$$

Nested control law

$$\delta(e_2, q, \alpha) = W_1 \left(q - \underbrace{W_2(e_1, \alpha, \delta)}_{\text{outer-loop actor}}, q, \alpha \right) \quad (14)$$

inner-loop actor

C. Inner-loop agent

The inner-loop agent aims to learn the control-surface deflection for the pitch-rate reference tracking. Equations 1 show that the action δ introduces a non-minimum-phase effect, whereby the control-surface deflection may unintentionally influence α -dynamics. This is a key motivation for adopting a cascaded control structure, which isolates the non-minimum-phase effect from the lower-level agent's training process. As a result, the agent is prevented from attempting to control angle-of-attack through the control-surface deflection.

Figure 2 shows the network structures. The critic network takes as input the pitch rate q_t and the tracking error $e_{q(t)}$. The output is the estimated value function $\hat{V}_2(t)$, with an absolute value activation applied at the output layer to ensure its positive definiteness. The actor network utilizes an additional input α to account for dynamic coupling in model 1. The output is the control surface deflection. A scaled $\tanh(\cdot)$ activation function is applied to constrain the action within actuator limits.

1) *Critic*: The critic is updated through TD learning to minimize a loss function:

$$L_t^{C2} = \frac{1}{2} \delta_{2(t)}^T \delta_{2(t)} \quad (15)$$

where $\delta_{2(t)} = c_{2(t)} + \gamma \hat{V}_{2\text{target}(t+1)} - \hat{V}_{2(t)}$ is the TD error, $c_{2(t)} = e_{2(t+1)}^2 + b\delta_t^2$ is the one-step cost, $\hat{V}_{2\text{target}}$ is a target critic.

2) *Actor*: The actor is trained to minimize the estimated state-value function:

$$L_t^{A2} = c_{2(t)} + \gamma \hat{V}_{2\text{target}(t+1)} \quad (16)$$

$$\delta^*(q_t, e_{2(t)}, \alpha_t) = \arg \min_{\delta_t} L_t^{A2} \quad (17)$$

The updates of networks are seen in Appendix VII-C.

The gradients of updating inner-loop critic and actor are constructed as follows.

Rewrite the loss L_t^{A2} :

$$L_t^{A2} = e_{2(t)}^2 + bu^2(t) + \gamma \hat{V}_{2\text{target}}(e_{t+1}, q_{t+1}, \alpha_{t+1}) \quad (18)$$

Its gradient with respect to inner-loop actor weights is

$$\begin{aligned} \frac{\partial L_t^{A2}}{\partial w} &= \frac{\partial L_t^{A2}}{\partial \delta} \frac{\partial \delta}{\partial w} \\ &= \left(2b\delta + \frac{\partial \hat{V}_{2\text{target}}}{\partial q_{t+1}} \frac{\partial q_{t+1}}{\partial \delta_t} \right) \frac{\partial \delta}{\partial w} \\ &= \left(2b\delta + \frac{\partial \hat{V}_{2\text{target}}}{\partial q_{t+1}} \hat{G}_{t-1}^2 \right) \frac{\partial \delta}{\partial w} \end{aligned} \quad (19)$$

3) *Training*: The separate policy training indicates the outer-loop and inner-loop actors are trained separately for angle-of-attack tracking control and pitch rate tracking control. The inner-loop actor minimizes a summed quadratic cost c_2 that measures the performance of pitch rate tracking. This process does not take the performance of angle-of-attack tracking into account (reflected as the critic does not use e_1 as input). The outer-loop actor is not involved in this process. The sample fed to the inner-loop agent is $(e_{2(t)}, q_t, \alpha_t, \delta_t, e_{2(t+1)}, q_{t+1})$, where α_t aims to attenuate the dynamics $f_2(x_1)$. In this case, the environment can be seen as the e_2 -dynamics. In the inner-loop training, the sample $(\delta_t, q_t, q_{\text{ref}(t)}, q_{t+1}, q_{\text{ref}(t+1)}, \alpha_{t+1})$ is fed to the agent to train critic and actor. The outer-loop actor gradient is generated through the inner-loop actor.

D. Outer-loop agent

The outer-loop agent aims to learn a pitch rate reference for angle-of-attack tracking control. Figure 1 shows the network topology as a single-hidden-layer perception. The critic takes as input α_t , the tracking error $e_{1(t)}$ and q . Its output is the estimated value function $\hat{V}_1(t)$, with an absolute value activation function $\text{abs}(\cdot)$ applied at the output layer to ensure positive definiteness. The actor uses an additional input δ_t to account for the non-minimum phase dynamics in the α -dynamics (see Equations 1). It outputs the virtual pitch rate command $q_{\text{ref}(t)}$, constrained by a scaled $\text{tanh}(\cdot)$ activation function to satisfy action constraints. The target critic and actor share the same structures as the critic and actor.

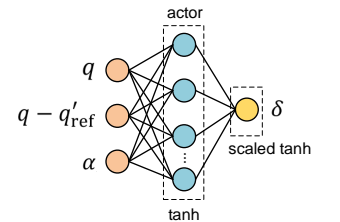
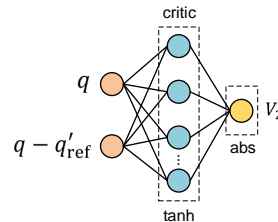
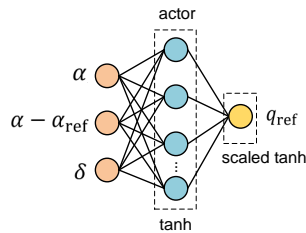
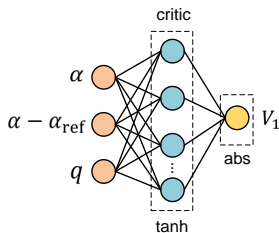


Fig. 1: Networks of outer-loop agent.

Fig. 2: Networks of inner-loop agent.

1) *Critic*: The critic is updated through Time-Difference (TD) learning to minimize a loss function:

$$L_t^{C1} = \frac{1}{2} \delta_{1(t)}^T \delta_{1(t)} \quad (20)$$

where $\delta_{1(t)} = c_{1(t)} + \gamma \hat{V}_{1\text{target}(t+1)} - \hat{V}_{1(t)}$ is the TD error, $c_{1(t)} = e_{1(t)}^2 + aq_{\text{ref}(t)}^2$ is the one-step cost function, $\hat{V}_{1\text{target}}$ is a target critic used to delay the weight updates and stabilize the learning process.

2) *Actor*: The actor is updated to minimize the estimated state-value function

$$L_t^{A1} = c_1(t) + \gamma \hat{V}_{1\text{target}(t+1)} \quad (21)$$

$$v^*(\alpha_t, e_{\alpha(t)}, \delta_t) = \arg \min_{v_t} L_t^{A1} \quad (22)$$

The updates of networks are seen in Appendix VII-B.

3) *Training*: In the outer-loop actor training, the action q_{ref} has to go through the inner-loop actor to generate an action δ to interact with the system. This implies that the outer-loop actor is interacting with an extended system that includes the inner-loop actor. The effect of the inner-loop actor can be seen as an equivariant control effectiveness for the outer-loop actor interacting with the system (see Equation 14). The sample used to feed the outer-loop actor is $(e_{1(t)}, \alpha_t, q_t, \delta_t, q_{\text{ref}}, e_{1(t+1)}, \alpha_{t+1}, q_{t+1})$.

In the training of the outer-loop agent, the weights of the inner loop actor is fixed.

Rewrite the loss L_t^{A1} :

$$L_t^{A1} = e_1^2(t) + a q_{\text{ref}}^2(t) + \gamma \hat{V}_{1\text{target}}(e_{1(t+1)}, \alpha_{t+1}, q_{t+1}) \quad (23)$$

Its gradient with respect to the outer-loop actor weights is

$$\begin{aligned} \frac{\partial L_t^{A1}}{\partial w} &= \left(2a q_{\text{ref}} + \gamma \frac{\partial \hat{V}_{1\text{target}}}{\partial q_{t+1}} \frac{\partial q_{t+1}}{\partial \delta_t} \frac{\partial \delta_t}{\partial q_{\text{ref}}} \right) \frac{\partial q_{\text{ref}}}{\partial w} \\ &= \left(2a q_{\text{ref}} + \gamma \frac{\partial \hat{V}_{1\text{target}}}{\partial q_{t+1}} \hat{G}_{t-1}^2 \frac{\partial \delta_t}{\partial q_{\text{ref}}} \right) \frac{\partial q_{\text{ref}}}{\partial w} \end{aligned} \quad (24)$$

where the gradient $\frac{\partial \delta_t}{\partial q_{\text{ref}}}$ is constructed through the inner-loop actor.

Remark 2. Only the control effectiveness G_{t-1}^1 is not needed to update the actor, since the control surface deflection goes to the pitch rate first.

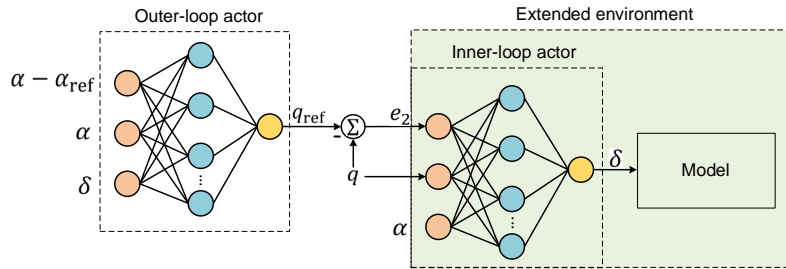


Fig. 3: Structure of the cascaded actor. The weights of the outer-loop actor are trained to generate a pitch rate reference, fed to the inner-loop actor. The weights of the inner-loop actor is trained to track the pitch rate reference, regardless of the angle-of-attack tracking error. Compared to a monolithic actor for end-to-end control, the cascaded structure introduces an explicit pitch-rate reference that defines a subtask for regularizing the angle-of-attack tracking error. This explicit reference provides a clear command for rate control, thereby improving the dynamic response of the control system.

V. ACTION-SMOOTHENING TECHNIQUES

This section introduces two action-smoothing techniques: policy regularization for temporal smoothness and a low-pass filter. The first technique regularizes the actor to produce slowly varying actions during training, while the second filters high-frequency signals of the pitch rate reference and thereby indirectly smooths the control-surface deflection.

A. Policy regularization for temporal action smoothness

The temporal smoothness of actions measures how much the action changes when the actor input changes. For the outer-loop and inner-loop actors, the measures are defined as

$$L_{1(t)}^{TS} = |v_{t+1} - v_t| \tag{25}$$

$$L_{2(t)}^{TS} = |\delta_{t+1} - \delta_t| \tag{26}$$

To reduce computational load in online learning, a single sample is used at each policy update step to compute the temporal smoothness loss. This contrasts with using a minibatch of samples to compute the smoothness loss in offline settings [29].

The multi-objective optimization frameworks can be formulated as

$$v^*(t) = \arg \min_{v_t} \left(c_{1(t)} + \gamma \hat{V}_{1\text{target}(t+1)} + \lambda_1 L_{1(t)}^{TS} \right) \tag{27}$$

$$\delta^*(t) = \arg \min_{\delta_t} \left(c_{2(t)} + \gamma \hat{V}_{2\text{target}(t+1)} + \lambda_2 L_{2(t)}^{TS} \right) \tag{28}$$

where λ_1, λ_2 are weights of smoothness losses.

B. Low-pass filter

A low-pass filter is used to smoothen the pitch rate reference q_{ref} , which is formulated as a second-order dynamics as [30]

$$\begin{aligned} \dot{d}_1 &= d_2 \\ \dot{d}_2 &= -2\zeta\omega_n d_2 - \omega_n^2 (d_1 - q_{\text{ref}}) \end{aligned} \tag{29}$$

where d_1, d_2 are filtered signal and its differentiation, ω_n is the natural frequency, ζ is the damping factor.

Remark 3. Using a filter in a cascaded learning control system violates the Markov assumption of the state transitions when the filter states are not included as part of the environment state. This is manifested by both the critic and the actor omitting the filter states from their inputs. During gradient backpropagation, the filter causes gradients to be delayed by two time steps. To avoid this delay effect, this paper excludes the filter during policy training and applies it only in the actor’s forward propagation.

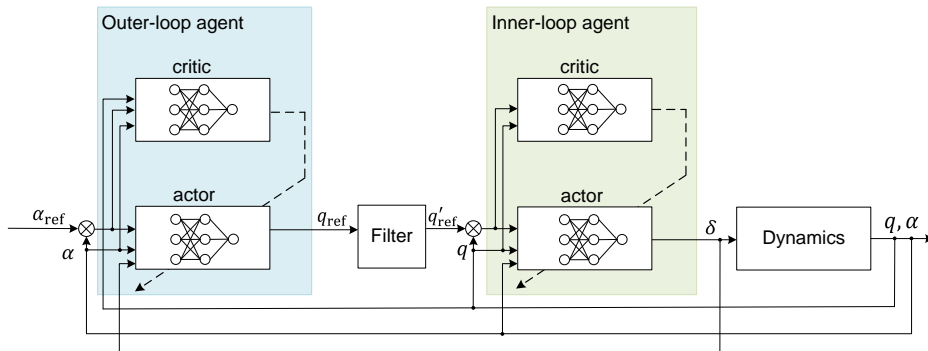


Fig. 4: Structure of the cascaded online learning flight control system.

VI. SIMULATION

This section provides simulation results of cascaded online learning flight control systems using action smoothness conditioning techniques. The aerial vehicle dynamics are numerically simulated through the fourth-order Runge Kutta method. The actuator dynamics are modeled as a first-order system $\tau \dot{\delta}_t + \delta_t = \delta_{c(t)}, \tau = 0.005$. To constrain actions, the actors are scaled to $20^\circ/\text{s}$ and 20° . The reference of angle-of-attack is set as $\alpha_{\text{ref}(t)} = 10^\circ \sin(\frac{2\pi}{T}t), T = 10\text{s}$. The hyperparameters of the RL agents are listed in Table II. The baseline control system does not use either of action-smoothing techniques. We consider the tracking control performance in aspects of tracking errors, action smoothness, saturation level of activation function, actor sensitivity and one-step costs.

TABLE II: Hyperparameters of RL agents

Parameter	Outer-loop Agent	Lower-level Agent 2
critic learning rate η_{C_1}, η_{C_2}	0.1	0.1
actor learning rate η_{A_1}, η_{A_2}	5×10^{-7}	10^{-7}
discount factor γ	0.6	0.6
delay factor τ	1	1
policy iteration number at each time step	3	3
hidden layer size	7	7
critic hidden-layer activation function	tanh	tanh
critic output layer activation function	abs	abs
actor activation function	tanh	tanh
optimizer	Adam	Adam
control weight b	5×10^{-6}	10^{-5}
smoothness loss weight λ_1, λ_2	9.3×10^{-4}	10^{-5}
loss thresholds for terminating critic training	2.5×10^{-4}	5×10^{-5}
maximal steps of critic and actor updates	50	50

A. Temporal-smoothed control system

1) *Tracking control*: Figure 5 shows tracking control performance of the baseline control system and temporal-smoothened control system. The baseline control system owns sever oscillations of states and actions, degrading the convergence of tracking error, which finally diverge. In contrast, the temporal-smoothened control system promotes smoother control behaviors and improves convergence of tracking errors, by penalizing the temporal variations of actions. Figure 6 shows that the critic parameters converge to their sub-optimum within 10s. The critic parameters of the baseline control system continue to oscillate in response to tracking errors. The growth of actor parameters is slowed down in temporally smoothed system as the application of TS losses stabilize tracking errors.

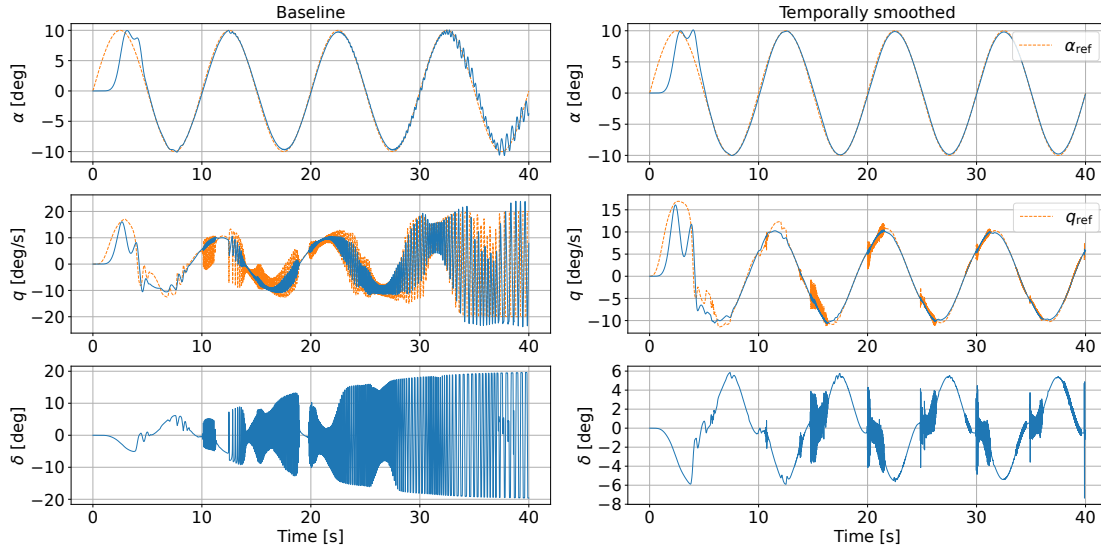


Fig. 5: Tracking control performance.

Figures 7 and 8 compare details of the pitch rate reference and control surface deflection, respectively. The frequency-domain characteristics are visualized using the Fast Fourier Transform (FFT), which converts action series in the time domain into a frequency-domain representation. The amplitude of q_{ref} reduces in a significant extension without losing tracking performance. The signals of q_{ref} within 100 Hz are effectively filtered using TS losses. Similar results are observed for control surface deflection. A reason for the oscillation of δ lies in that the switching q_{ref} causes switching tracking error e_2 , as an input of the lower-level actor.

In the authors' opinion, using a TS loss can be understood as a prior information about the behavior of the expected control policy, i.e., using smooth actions to interact with the system. A TS loss discourages RL agents from producing aggressive actions. Such actions may lead to saturation of actors' activation functions. This saturation further lead to vanishing of gradients, making it difficult to go back to the gradient-sensitive zone. This indicates that the agent does not easily 'unlearn' a low-gain control policy once it learns a high-gain control policy. Consequently, the actors become stubborn in adjusting gains according to tracking errors, which leads to final divergence of tracking error. This process is exhibited in Figure 5.

2) *Action increment*: The one-step increment of virtual pitch rate reference is defined as

$$\Delta q_{ref(t+1)} = |q_{ref(t+1)} - q_{ref(t)}| \tag{30}$$

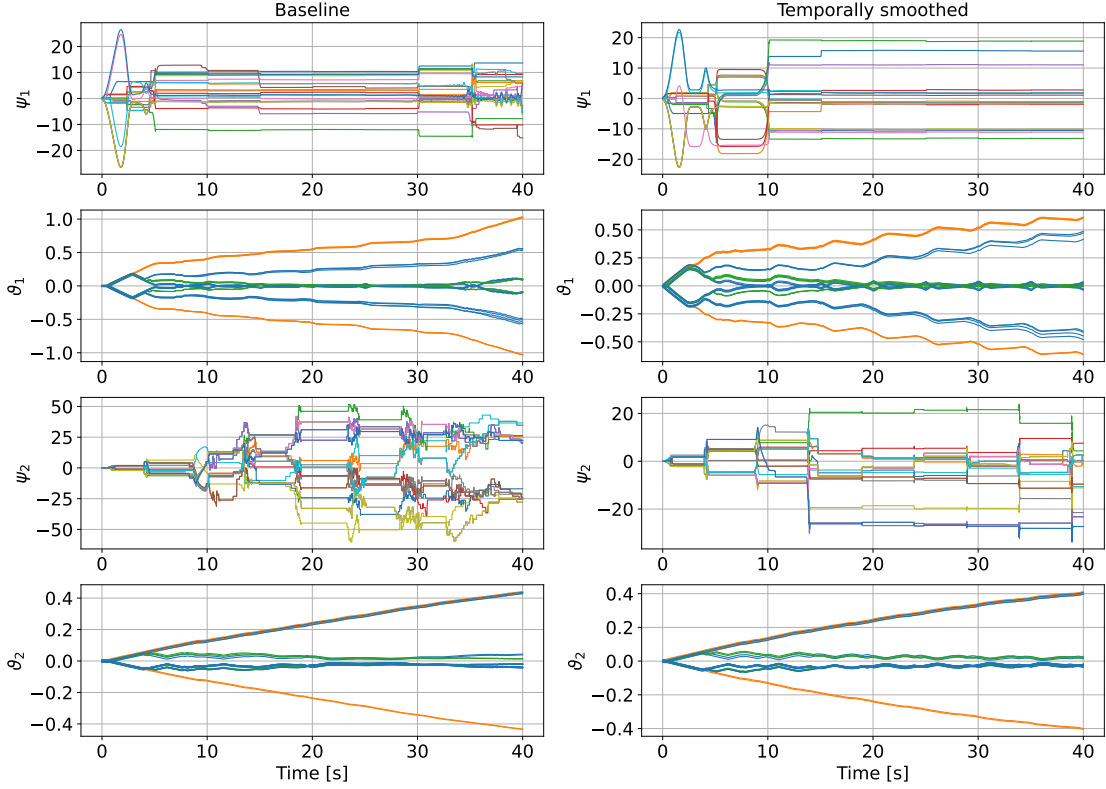


Fig. 6: Critic and actor parameters.

where $q_{\text{ref}(t)}, q_{\text{ref}(t+1)}$ are actor outputs in $t + 1, t$ and are defined as

$$q_{\text{ref}(t+1)} = W^{\vartheta_1}(e_{\alpha(t+1)}, \alpha_{t+1}, \delta_{t+1}) \quad (31)$$

$$q_{\text{ref}(t)} = W^{\vartheta_1}(e_{\alpha(t)}, \alpha_t, \delta_t) \quad (32)$$

The one-step increment of control surface deflection is

$$\Delta\delta_{t+1} = |\delta_{t+1} - \delta_t| \quad (33)$$

where δ_{t+1}, δ_t are actor outputs in $t + 1, t$ and are defined as:

$$\delta_{t+1} = W^{\vartheta_2}(e_{q(t+1)}, q_{t+1}, \alpha_{t+1}) \quad (34)$$

$$\delta_t = W^{\vartheta_2}(e_{q(t)}, q_t, \alpha_t)$$

Figure 9 compares action increments. The TS loss used for the outer-loop agent reduces the amplitude of action increment to $|\Delta q_{\text{ref}(t+1)}| \leq 0.5$ deg/s. For the lower-level agent, the amplitude of $|\Delta\delta(t)|$ is restricted by actuator limits. This improvement demonstrates the disadvantage of the baseline control system that it does not penalize aggressive actions so that it learns a bang-bang control strategy to reduce tracking errors, while the TS loss penalizes fast changes of actions so that a low-gain control law is learned.

3) *Activation function*: The saturation of an activation function $\tanh(\cdot)$ indicates its output approaches the maximum or minimum value due to large amplitude of input (see Figure 10). Meantime, its gradient vanishes and finally approaches zero. The vanishing gradient leads to slow-pace learning of control policy through gradient descent approaches. A worse effect is that a saturated activation function outputs maximum or minimum actions in response to tracking errors, resulting in a bang-bang control effect. This bang-bang control effect will degrade tracking control performance and system stability.

A bang-bang control policy can be learned through an overly aggressive process of policy learning. This process occurs for two main reasons: (1) a large learning rate. A large learning rate makes the actor's weights updated with large increments, pushing the activation function into its saturation zone. (2) Inadequately weighting in the loss function. A loss function that underemphasizes the control effort may lead to the actor learning to generate large control actions in response to tracking errors, without properly accounting for control effort. These large actions typically arise from saturated activation functions.

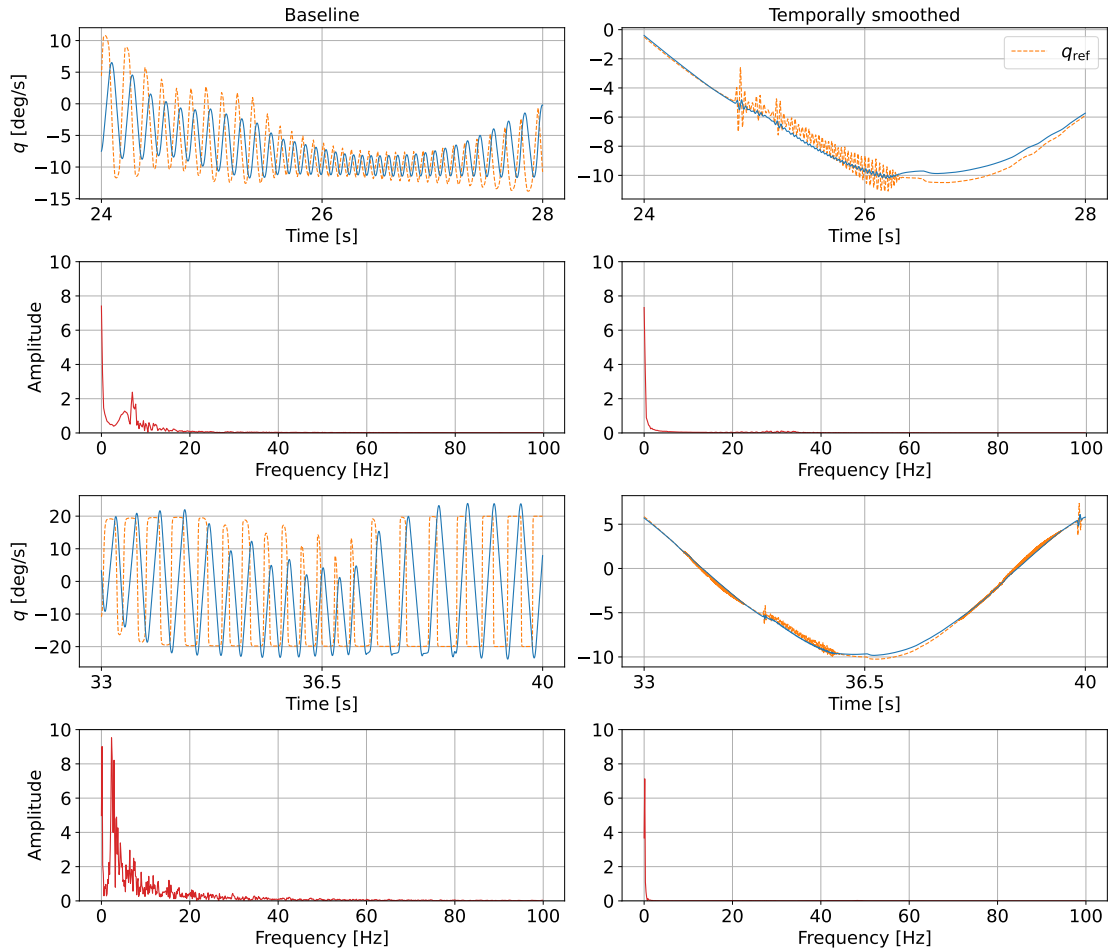


Fig. 7: Pitch rate in selected intervals.

Moreover, these aggressive learning behaviors persist even as the tracking error decreases, continuing to degrade the control performance.

Figure 10 shows the dynamical saturation level of activation functions in output layers of actors. The baseline control system eventually makes the inputs of $\tanh(\cdot)$ reach to intervals $[-4,-2]$, $[2,4]$ (the outer-loop actor), and $[-3,-2]$, $[2,3]$ (the lower-level actor). In these intervals, the derivative of $\tanh(\cdot)$ is less than 0.1, providing slight gradients for actor training. As a comparison, the temporal-smoothened control system avoids the saturation even starting with the same settings. The inputs are kept within 'unsaturated' intervals $[-2,2]$ (the outer-loop actor) and $[-0.5,0.5]$ (the lower-level actor). This demonstrates the effectiveness of TS losses in avoiding saturation of $\tanh(\cdot)$.

4) *Actor sensitivity*: The sensitivity of an actor indicates how much and in what direction the output will change if the input slightly increases [34]. The high sensitivity may cause the actor to overreact to state variations and overcorrect the tracking error. This is also correlated to robustness of the actor against sensor noise and uncertainties.

The sensitivity measures for actors are defined as

$$K_{1(t)} = \frac{\partial q_{\text{ref}(t)}}{\partial e_{\alpha(t)}} \quad (35)$$

$$K_{2(t)} = \frac{\partial \delta(t)}{\partial e_{q(t)}} \quad (36)$$

where $K_{1(t)}$, $K_{2(t)}$ are sensitivity measures.

The pitch rate reference and its sensitivity measure are related as

$$\begin{aligned} & |q_{\text{ref}(t+1)} - q_{\text{ref}(t)}| \\ & \approx |K_{1(t)}(e_{\alpha(t+1)} - e_{\alpha(t)})| \\ & = |K_{1(t)}| \cdot |e_{\alpha(t+1)} - e_{\alpha(t)}| \end{aligned} \quad (37)$$

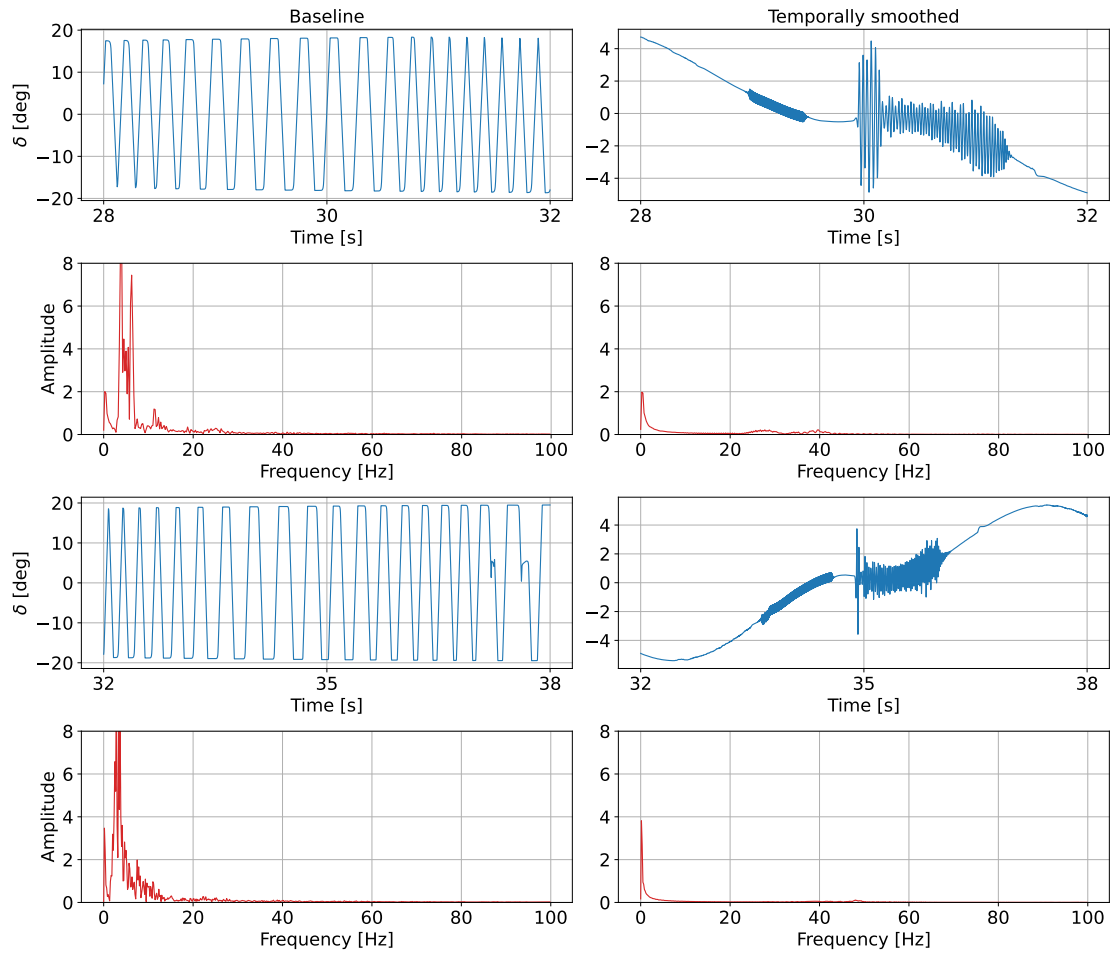


Fig. 8: Control surface deflection in selected intervals.

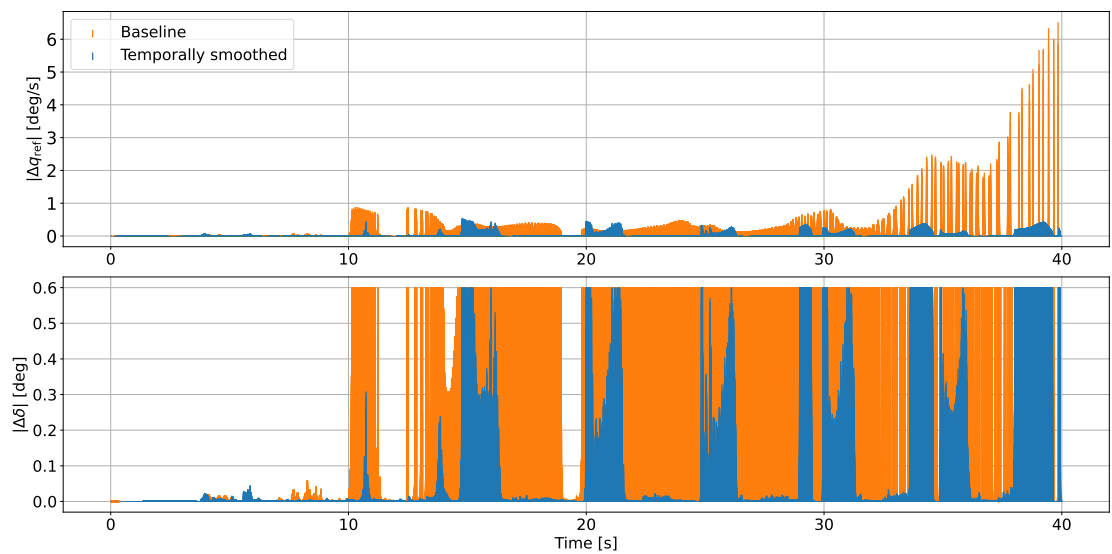


Fig. 9: Increments of actions generated from the outer-loop actor and the inner-loop actor.

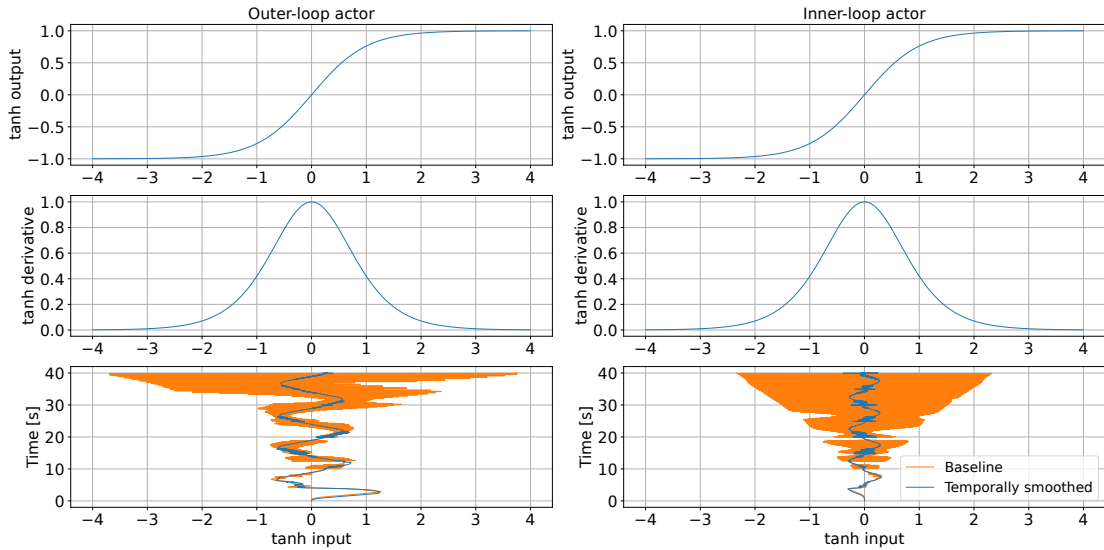


Fig. 10: Input of the activation function $\tanh(\cdot)$ in output layers of actors.

Similarly, the control surface deflection and its sensitivity measure are related as

$$\begin{aligned}
 & |\delta_{(t+1)} - \delta_{(t)}| \\
 & \approx |K_{2(t)}(e_{q(t+1)} - e_{q(t)})| \\
 & = |K_{2(t)}| \cdot |e_{q(t+1)} - e_{q(t)}|
 \end{aligned} \tag{38}$$

Remark 4. Equations 37, 38 show that the increments of (virtual) action can be reduced through reducing sensitivity. This is demonstrated in Figure 11.

Figure 11 compares sensitivity measures. The baseline control system shows oscillations, indicating the actor is significantly sensitive to error variants. The temporal-smoothened control system shows reduced oscillations because the TS losses penalize the increments of actions. The action increments are determined by actor sensitivity.

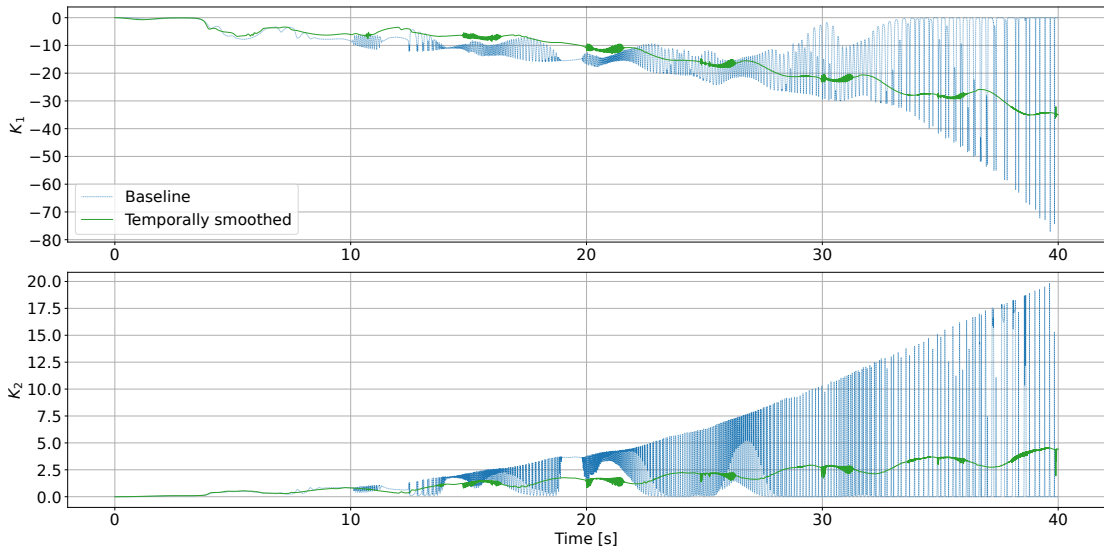


Fig. 11: Sensitivity measures.

5) *Challenges:* Although the policy regularization for temporal smoothness helps the actor produce smoother actions, the tuning of actor weight tuning is empirical. An inappropriately large weight slows down the process of actor training, while an inappropriately small weight may show degraded smoothness effect. The selection of an appropriate weight for the temporal smoothness loss remains an unresolved issue. On the other hand, Figure 12 shows that the TS loss does not eliminate small-amplitude, high-frequency oscillations in pitch rate reference and control surface deflection, since its effect diminishes when the magnitude of action increments is small. In this situation, a low-pass filter shows its ability of filtering high-frequency

commands in frequency domain perspective, and thus reduces these state oscillations. Meanwhile, incorporating a low-pass filter into the flight control system does not interfere with the training of the actors.

B. Command-filtered and temporal-smoothed control system

We introduce a low-pass filter into the cascaded online learning flight control system, which has been demonstrated effective in filtering pitch rate reference in [5]. The parameters of the filter are given as $\zeta = 0.7$, $\omega_0 = 20\text{rad/s}$ (check the units).

1) *Tracking control*: Figure 12 compares angle-of-attack tracking performance between a temporal-smoothed control system and a temporal-smoothed control system with a filter. It is shown that the filter is capable of attenuating high-frequency oscillations in pitch rate reference and control surface deflection. Figure 13 presents detailed comparisons of the pitch-rate reference over short time periods. The signals of q_{ref} in 10-40Hz are effectively eliminated by a filter. Figure 14 provides detailed comparisons on δ over short time periods. The signals of δ in 10-40Hz are effectively attenuated. This performance is achieved through a specific set of filter parameters.

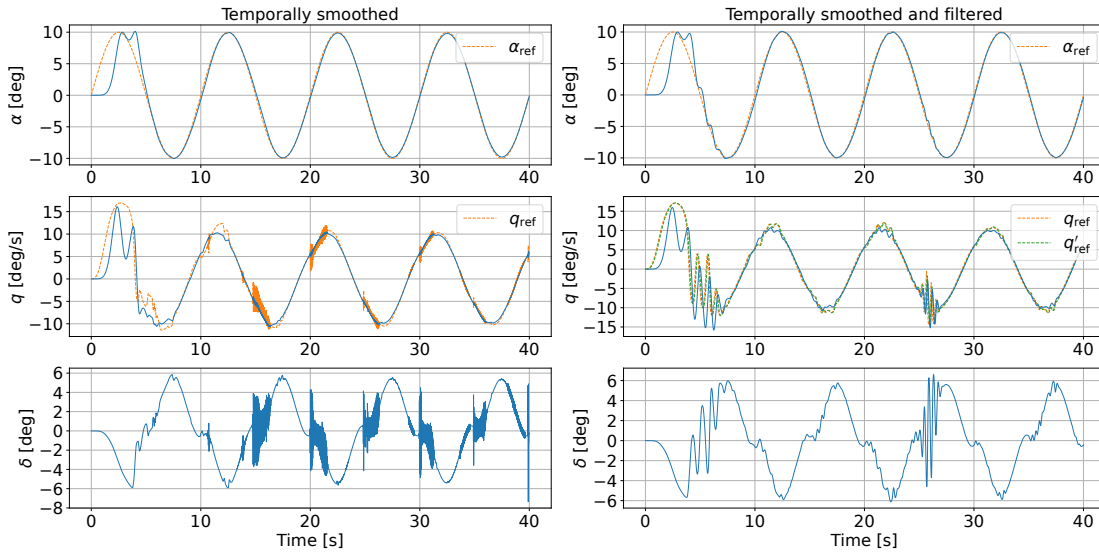


Fig. 12: Tracking performance comparison.

2) *Activation function*: Figure 15 shows the dynamical saturation level of the activation function $\tanh(\cdot)$ in the output layer of actors. Both the temporal-smoothened and temporal-smoothened with a filter methods prevent saturation of $\tanh(\cdot)$, ensuring its gradient remains within the sensitive, non-vanishing region, supporting effective policy learning.

3) *Actor sensitivity*: Figure 16 compares the sensitivity measures $K_1(t)$ and $K_2(t)$. The results show that the use of a filter slows the growth of the measures and reduces their oscillations, contributing to a more robust controller.

VII. CONCLUSION

We introduced two action-smoothening techniques into the cascaded online learning flight control system: temporal policy regularization and low-pass filter. The temporal policy regularization is verified through simulation to reduce the amplitude of pitch rate reference and control surface deflection. The low-pass filter is verified capable of removing the high-frequency signals of pitch rate reference, which cannot be accomplished by only using temporal policy regularization. The combination of these two methods enables a sufficient-level action smoothness during online learning.

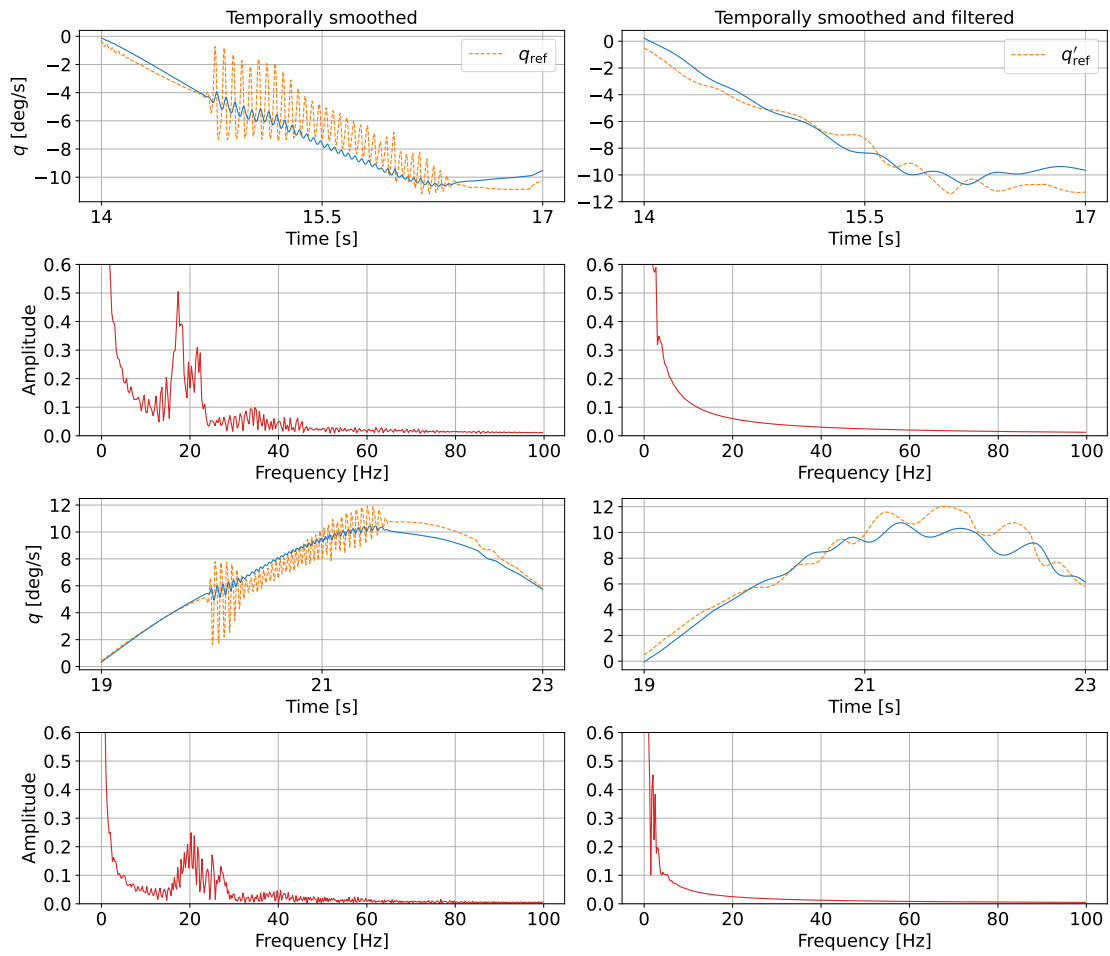


Fig. 13: Pitch rate in selected intervals.

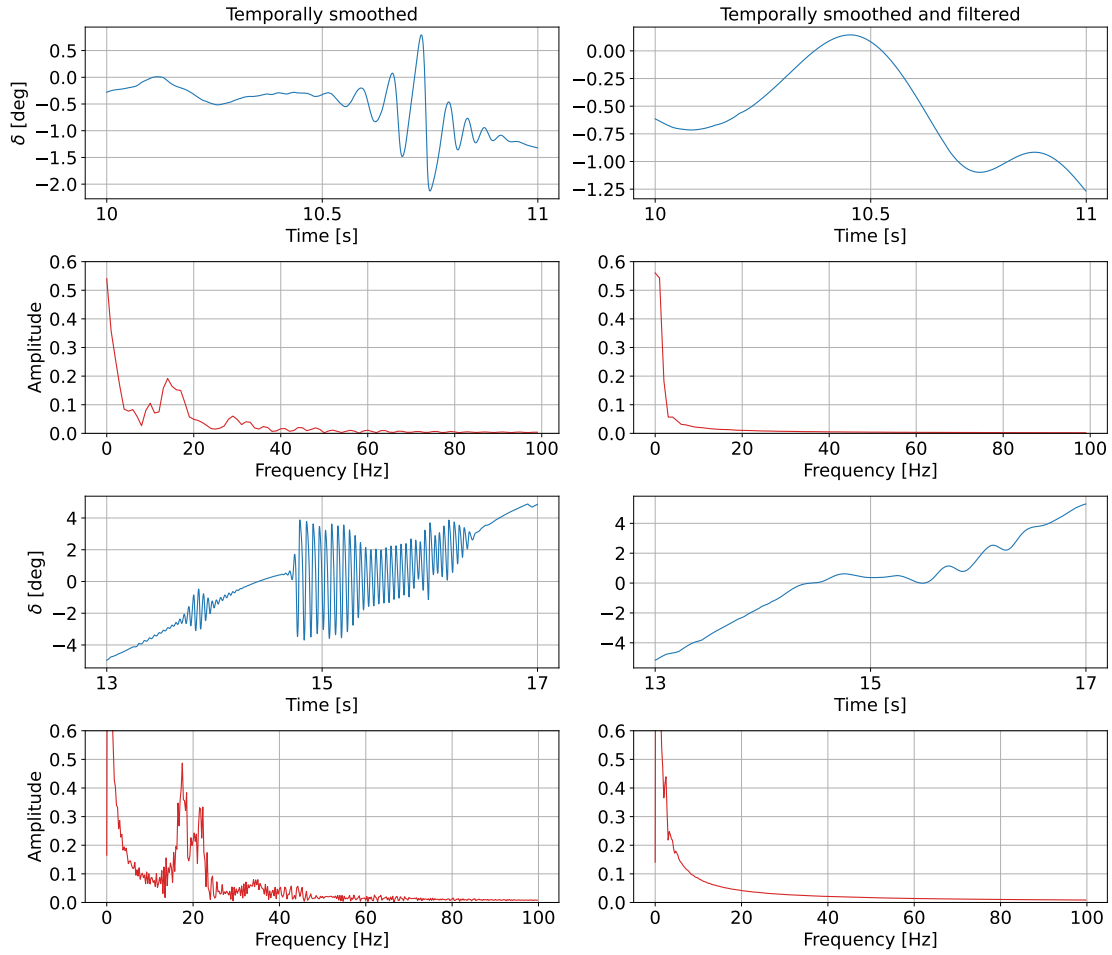


Fig. 14: Control surface deflection in selected intervals.

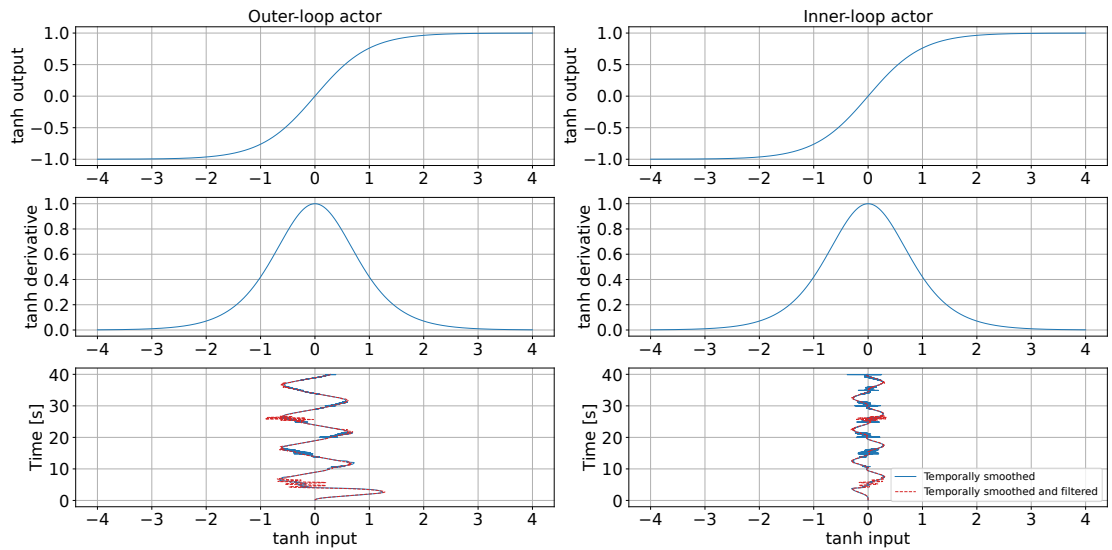


Fig. 15: Input of the activation function $\tanh(\cdot)$ in the output layer of actors.

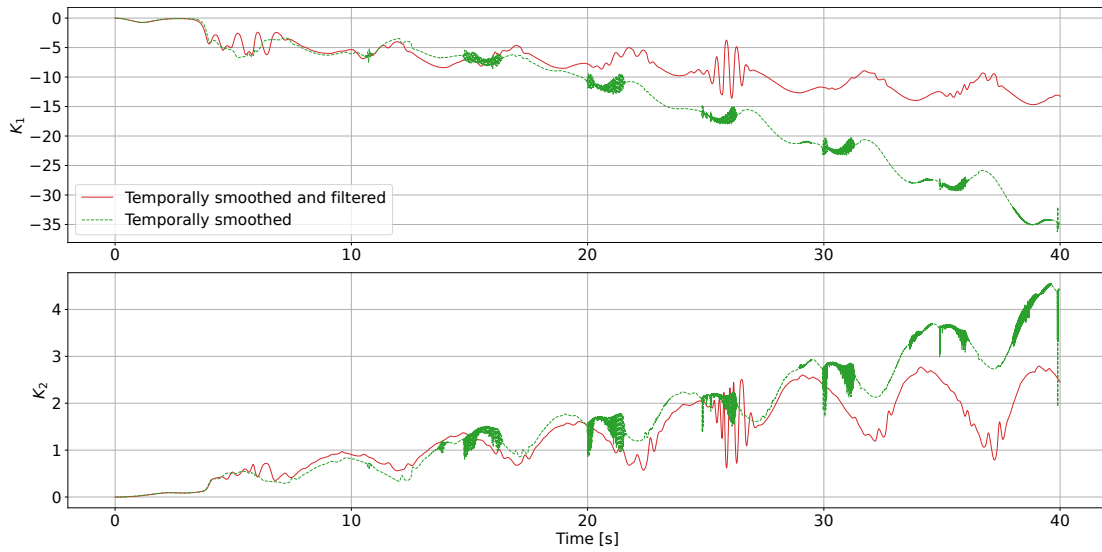


Fig. 16: Sensitivity measures.

APPENDIX

A. Derivation of incremental model

Taking the Taylor expansion of systems 1:

$$\begin{aligned}\alpha_{t+1} &= \alpha_t + F_{t-1}^1(\alpha_t - \alpha_{t-1}) + G_{t-1}^1(q_t - q_{t-1}) \\ &\quad + O[(\alpha_t - \alpha_{t-1})^2, (q_t - q_{t-1})^2] \\ q_{t+1} &= q_t + F_{t-1}^2(q_t - q_{t-1}) + G_{t-1}^2(\delta_t - \delta_{t-1}) \\ &\quad + O[(q_t - q_{t-1})^2, (\delta_t - \delta_{t-1})^2]\end{aligned}\tag{39}$$

where

$$\begin{aligned}F_{t-1}^1 &= \frac{\partial h_1[\alpha_t, \delta_t, q_t]}{\partial \alpha_t} \Big|_{\alpha_{t-1}, \delta_{t-1}, q_{t-1}} \\ G_{t-1}^1 &= \frac{\partial h_1[\alpha_t, \delta_t, q_t]}{\partial q_t} \Big|_{\alpha_{t-1}, \delta_{t-1}, q_{t-1}} \\ F_{t-1}^2 &= \frac{\partial h_2[\alpha_t, \delta_t, q_t]}{\partial q_t} \Big|_{\alpha_{t-1}, \delta_{t-1}, q_{t-1}} \\ G_{t-1}^2 &= \frac{\partial h_2[\alpha_t, \delta_t, q_t]}{\partial q_t} \Big|_{\alpha_{t-1}, \delta_{t-1}, q_{t-1}}\end{aligned}\tag{40}$$

and $O(\cdot)$ represents higher-order terms that can be ignored if the time step t is sufficiently small.

Define state increments and control increment as

$$\begin{aligned}\Delta \alpha_t &= \alpha_t - \alpha_{t-1} \\ \Delta q_t &= q_t - q_{t-1} \\ \Delta \delta_t &= \delta_t - \delta_{t-1}\end{aligned}\tag{41}$$

Therefore, the incremental model can be formulated as

$$\begin{aligned}\Delta \alpha_{t+1} &= F_{t-1}^1 \Delta \alpha_t + G_{t-1}^1 \Delta q_t \\ \Delta q_{t+1} &= F_{t-1}^2 \Delta q_t + G_{t-1}^2 \Delta \delta_t\end{aligned}\tag{42}$$

B. Higher-level agent's critic and actor update

1) *Critic*: The gradient of $L_t^{C_1}$ with respect to ψ_1 is

$$\begin{aligned}\frac{\partial L_t^{C_1}}{\partial \psi_{1(t)}} &= \frac{\partial L_t^{C_1}}{\partial \delta_{1(t)}} \frac{\partial \delta_{1(t)}}{\partial \psi_{1(t)}} \\ &= -\delta_{1(t)} \frac{\partial \hat{V}_1(\alpha_t, e_{\alpha(t)})}{\partial \psi_{1(t)}}\end{aligned}\tag{43}$$

The parameter set ψ_1 is updated as

$$\psi_{1(t+1)} = \psi_{1(t)} - \eta_{C_1} \frac{\partial L_t^{C_1}}{\partial \psi_{1(t)}}\tag{44}$$

where η_{C_1} is the learning rate.

2) *Target Critic*: The target critic network is used to stabilize learning by delaying the updates:

$$\psi'_{1(t+1)} = \tau \psi_{1(t+1)} + (1 - \tau) \psi'_{1(t)}\tag{45}$$

where τ is delay factor τ , ψ'_1 is the parameter set of target critic.

3) *Actor*: The gradient of L_t^{A1} with respect to ϑ_1 is

$$\begin{aligned}
 \frac{\partial L_t^{A1}}{\partial \vartheta_{1(t)}} &= \frac{\partial \left[c_1(\hat{e}_{\alpha(t+1)}, q_t) + \gamma \hat{V}_1(\hat{\alpha}_{t+1}, \hat{e}_{\alpha(t+1)}) \right]}{\partial \vartheta_{1(t)}} \\
 &= \left[\frac{\partial c_1(\hat{e}_{\alpha(t+1)}, q_t)}{\partial \hat{\alpha}_{t+1}} + \gamma \frac{\hat{V}_1(\hat{\alpha}_{t+1}, \hat{e}_{\alpha(t+1)})}{\partial \hat{\alpha}_{t+1}} \right] \\
 &\quad \frac{\partial \hat{\alpha}_{t+1}}{\partial q_{\text{ref}}(t)} \frac{\partial q_{\text{ref}}(t)}{\partial \vartheta_{1(t)}} \\
 &= \left[\frac{\partial c_1(\hat{e}_{\alpha(t+1)}, q_t)}{\partial \hat{\alpha}_{t+1}} + \gamma \frac{\hat{V}_1(\hat{\alpha}_{t+1}, \hat{e}_{\alpha(t+1)})}{\partial \hat{\alpha}_{t+1}} \right] \\
 &\quad \hat{G}_{t-1}^1 \frac{\partial q_{\text{ref}}(t)}{\partial \vartheta_{1(t)}}
 \end{aligned} \tag{46}$$

The parameter set ϑ_1 is updated as

$$\vartheta_{1(t+1)} = \vartheta_{1(t)} - \eta_{A1} \frac{\partial L_t^{A1}}{\partial \vartheta_{1(t)}} \tag{47}$$

where η_{A1} is the learning rate.

From an algorithmic perspective, the update of ψ_t to ψ_{t+1} can be performed multiple times until the critic loss L_{critic} falls below a specified threshold. Subsequently, the update of ϑ_t to ϑ_{t+1} can also be repeated until the actor loss L_{actor} begins to reverse direction, indicating that ϑ_t is near a local optimum. These steps constitute one iteration of approximate value iteration. The approximate value iteration can be executed for multiple times at time step t .

C. Lower-level agent's critic and actor update

1) *Critic*: The gradient of L_t^{C2} with respect to ψ_2 is

$$\begin{aligned}
 \frac{\partial L_t^{C2}}{\partial \psi_2(t)} &= \frac{\partial L_t^{C2}}{\partial \delta_{2(t)}} \frac{\partial \delta_{2(t)}}{\partial \psi_2(t)} \\
 &= -\delta_{2(t)} \frac{\partial \hat{V}(q_t, e_q(t))}{\partial \psi_2(t)}
 \end{aligned} \tag{48}$$

The parameter set ψ_2 is updated as

$$\psi_2(t+1) = \psi_2(t) - \eta_{C2} \frac{\partial L_t^{C2}}{\partial \psi_2(t)} \tag{49}$$

where η_{C2} is the learning rate.

2) *Target Critic*: Target critic is used to stabilize the learning by slowing down the network update.

$$\psi'_{2(t+1)} = \tau \psi_{2(t+1)} + (1 - \tau) \psi'_{2(t)} \tag{50}$$

where τ is delay factor, ψ'_2 is parameter set of target critic.

3) *Actor*: The gradient of L_t^{A2} with respect to ϑ_2 is

$$\begin{aligned}
 \frac{\partial L_t^{A2}}{\partial \vartheta_{2(t)}} &= \frac{\partial \left[c_2(\hat{e}_{q(t+1)}, \delta_t) + \gamma \hat{V}_{2\text{target}}(\hat{q}_{t+1}, \hat{e}_{q(t+1)}) \right]}{\partial \vartheta_{2(t)}} \\
 &= \left[\frac{\partial c_2(\hat{e}_{q(t+1)}, \delta_t)}{\partial \hat{q}_{t+1}} + \gamma \frac{\hat{V}_{2\text{target}}(\hat{q}_{t+1}, \hat{e}_{q(t+1)})}{\partial \hat{q}_{t+1}} \right] \\
 &\quad \frac{\partial \hat{q}_{t+1}}{\partial \delta_{e(t)}} \frac{\partial \delta_{e(t)}}{\partial \vartheta_{2(t)}} \\
 &= \left[\frac{\partial c_2(\hat{e}_{q(t+1)}, \delta_t)}{\partial \hat{q}_{t+1}} + \gamma \frac{\hat{V}_{2\text{target}}(\hat{q}_{t+1}, \hat{e}_{q(t+1)})}{\partial \hat{q}_{t+1}} \right] \\
 &\quad \hat{G}_{t-1}^2 \frac{\partial \delta_{e(t)}}{\partial \vartheta_{2(t)}}
 \end{aligned} \tag{51}$$

The parameter set ϑ_2 is updated as

$$\vartheta_{2(t+1)} = \vartheta_{2(t)} - \eta_{A_2} \frac{\partial L_t^{A_2}}{\partial \vartheta_{2(t)}} \quad (52)$$

where η_{A_2} is the learning rate.

REFERENCES

- [1] J. D. Anderson *Fundamentals of Aerodynamics*. McGraw-Hill Series in Aeronautical and Aerospace Engineering. New York, USA: McGraw-Hill, 2017.
- [2] S. Sieberling, Q. P. Chu, and J. A. Mulder Robust Flight Control Using Incremental Nonlinear Dynamic Inversion and Angular Acceleration Prediction *Journal of Guidance, Control and Dynamics*, vol. 33, no. 6, pp. 1732–1742, 2010, doi: 10.2514/1.49978.
- [3] X. R. Wang, E. van Kampen, Q. P. Chu and P. Lu Stability Analysis for Incremental Nonlinear Dynamic Inversion Control *Journal of Guidance, Control and Dynamics*, vol. 42, no. 5, pp. 1116–1129, 2019, doi: 10.2514/1.G003791.
- [4] Z. C. Liu, Y. F. Zhang, and J. J. Liang and H. X. Chen Application of the Improved Incremental Nonlinear Dynamic Inversion in Fixed-Wing UAV Flight Tests *Journal of Aerospace Engineering*, vol. 35, no. 6, pp. 1–13, 2022, doi: 10.1061/(ASCE)AS.1943-5525.0001495.
- [5] Y. C. Wang, W. S. Chen, S. X. Zhang, J. W. Zhu and L. J. Cao Command-Filtered Incremental Backstepping Controller for Small Unmanned Aerial Vehicles *Journal of Guidance, Control, and Dynamics*, vol. 41, no. 4, pp. 952–965, 2018, doi: 10.2514/1.G003001.
- [6] X. R. Wang, E. van Kampen, Q. P. Chu and P. Lu Incremental Sliding-Mode Fault-Tolerant Flight Control *Journal of Guidance, Control, and Dynamics*, vol. 42, no. 2, pp. 244–259, 2019, doi: 10.2514/1.G003497.
- [7] W. H. Chen, J. Yang, L. Guo and S. H. Li Disturbance-Observer-Based Control and Related Methods—An Overview *IEEE Transactions on Industrial Electronics*, vol. 63, no. 2, pp. 1083–1095, 2016, doi: 10.1109/TIE.2015.2478397.
- [8] D. M. Acosta and S. S. Joshi Adaptive Nonlinear Dynamic Inversion Control of an Autonomous Airship for the Exploration of Titan *AIAA Guidance, Navigation and Control Conference and Exhibit*, Hilton Head, South Carolina, USA, August, 2007, doi: 10.2514/6.2007-6502.
- [9] E. J. J. Smeur, Q. P. Chu and G. H. E. de Croon Adaptive Incremental Nonlinear Dynamic Inversion for Attitude Control of Micro Air Vehicles *Journal of Guidance, Control, and Dynamics*, vol. 39, no. 3, pp. 450–461, 2016, doi: 10.2514/1.G001490.
- [10] B. Smit, T. S. C. Pollack and E. van Kampen Adaptive Incremental Nonlinear Dynamic Inversion Flight Control for Consistent Handling Qualities *AIAA SciTech 2022 Forum*, San Diego, CA&Virtual, USA, January, 2022, doi: 10.2514/6.2022-1394.
- [11] J. Harris, C. M. Elliott and G. S. Tallant L1 Adaptive Nonlinear Dynamic Inversion Control for the Innovative Control Effectors Aircraft *AIAA SciTech 2022 Forum*, San Diego, CA&Virtual, USA, January, 2022, doi: 10.2514/6.2022-0791.
- [12] L. Sonneveldt, Q. P. Chu and J. A. Mulder Constrained Adaptive Backstepping Flight Control: Application to a Nonlinear F-16/MATV Model *AIAA Guidance, Navigation and Control Conference and Exhibit*, Keystone, Colorado, USA, August, 2006, doi: 10.2514/6.2006-6413.
- [13] L. Sonneveldt, Q. P. Chu and J. A. Mulder Nonlinear Flight Control Design Using Constrained Adaptive Backstepping *Journal of Guidance, Control, and Dynamics*, vol. 30, no. 2, pp. 322–336, 2007, doi: 10.2514/1.25834.
- [14] Q. Hu, Y. Meng, C. L. Wang and Y. M. Zhang Adaptive Backstepping Control for Air-breathing Hypersonic Vehicles with Input Nonlinearities *Aerospace Science and Technology*, vol. 73, pp. 289–299, 2018, doi: 10.1016/j.ast.2017.12.001.
- [15] R. S. Sutton and A. G. Barto *Reinforcement Learning: An Introduction*. 6th edition, Sigma Series in Pure Mathematics. Cambridge, MA, USA: A Bradford Book, 2018.
- [16] Y. Zhou, E. van Kampen and Q.P. Chu Incremental Model Based Online Dual Heuristic Programming for Nonlinear Adaptive Control *Control Engineering Practice*, vol. 73, pp. 13–25, 2018, doi: 10.1016/j.conengprac.2017.12.011.
- [17] Y. Zhou, E. van Kampen and Q. P. Chu Incremental Approximate Dynamic Programming for Nonlinear Flight Control Design In *Proceedings of the EuroGNC 2015*, Toulouse, France, 2015.
- [18] Y. Zhou, E. van Kampen and Q. P. Chu Incremental Approximate Dynamic Programming for Nonlinear Adaptive Tracking Control with Partial Observability *Journal of Guidance, Control, and Dynamics*, vol. 41, no. 12, pp. 2554–2567, 2018, doi: 10.2514/1.G003472.
- [19] Y. Zhou, E. van Kampen and Q.P. Chu An Incremental Approximate Dynamic Programming Flight Controller Based on Output Feedback *AIAA Guidance, Navigation, and Control Conference*, San Diego, California, USA, January, 2016, doi: 10.2514/6.2016-0360.
- [20] B. Sun and E. van Kampen Incremental Model-Based Heuristic Dynamic Programming with Output Feedback Applied to Aerospace System Identification and Control *2020 IEEE Conference on Control Technology and Applications*, Montreal, QC, Canada, 2020, pp. 366-371, August, 2020, doi: 10.1109/CCTA41146.2020.9206261.
- [21] B. Sun and E. van Kampen Intelligent Adaptive Optimal Control Using Incremental Model-Based Global Dual Heuristic Programming Subject to Partial Observability *Applied Soft Computing*, vol. 103, pp. 1–15, 2021, doi: 10.1016/j.asoc.2021.107153.
- [22] B. Sun and E. van Kampen Reinforcement-Learning-Based Adaptive Optimal Flight Control with Output Feedback and Input Constraints *Journal of Guidance, Control, and Dynamics*, vol. 44, no. 9, pp. 1685–1691, 2021, doi: 10.2514/1.G005715.
- [23] B. Sun and E. van Kampen Event-Triggered Constrained Control Using Explainable Global Dual Heuristic Programming for Nonlinear Discrete-Time Systems *Neurocomputing*, vol. 468, pp. 452–463, 2022, doi: 10.1016/j.neucom.2021.10.046.
- [24] Y. Zhou, E. van Kampen and Q.P. Chu Incremental Model Based Heuristic Dynamic Programming for Nonlinear Adaptive Flight Control In *Proceedings of the International Micro Air Vehicles Conference and Competition*, Beijing, China, October, 2016, url: <https://www.imavs.org/papers/2016/25.pdf>.
- [25] Y. Zhou, E. van Kampen and Q. P. Chu Incremental Model based Online Heuristic Dynamic Programming for Nonlinear Adaptive Tracking Control with Partial Observability *Aerospace Science and Technology*, vol. 105, pp. 1–14, 2020, doi: 10.1016/j.ast.2020.106013.
- [26] S. Heyer, D. Kroezen and E. van Kampen Online Adaptive Incremental Reinforcement Learning Flight Control for a CS-25 Class Aircraft *AIAA Scitech 2020 Forum*, Orlando, FL, USA, October, 2020, doi: 10.2514/6.2020-1844.
- [27] L.G. Sun, C.C. de Visser, Q.P. Chu and W. Falkena Hybrid Sensor-Based Backstepping Control Approach with Its Application to Fault-Tolerant Flight Control *Journal of Guidance, Control, and Dynamics*, vol. 31, no. 1, pp. 59–71, 2014, doi: 10.2514/1.61890.
- [28] Y. Zhou, E. van Kampen and Q.P. Chu Launch Vehicle Adaptive Flight Control with Incremental Model Based Heuristic Dynamic Programming *International Astronautical Congress*, Adelaide, Australia, September, 2017.
- [29] S. Mysore, B. Mabsout, R. Mancuso and K. Saenko Regularizing Action Policies for Smooth Control with Reinforcement Learning *IEEE International Conference on Robotics and Automation*, Xi'an, China, October, 2021, doi: 10.1109/ICRA48506.2021.9561138.
- [30] A.N. Kalliny, A.A. El-Badawy and S.M. Elkhamsy Command-Filtered Integral Backstepping Control of Longitudinal Flapping-Wing Flight *Journal of Guidance, Control, and Dynamics*, vol. 41, no. 7, pp. 1556–1568, 2018, doi: 10.2514/1.G003267.
- [31] J.A. Farrell, M. Polycarpou, M. Sharma and W. Dong Command Filtered Backstepping *IEEE Transactions on Automatic Control*, vol. 54, no. 6, pp. 1391-1395, 2009, doi: 10.1109/TAC.2009.2015562.
- [32] R.A. Hull, D. Schumacher and Z.H. Qu Design and Evaluation of Robust Nonlinear Missile Autopilots from a Performance Perspective In *Proceedings of 1995 American Control Conference*, Seattle, WA, USA, June, 1995, doi: 10.1109/ACC.1995.529235.
- [33] P. J. Werbos Advanced Forecasting Methods for Global Crisis Warning and Models of Intelligence *General Systems*, vol. 22, pp. 25-38, 1977, url: <https://gwern.net/doc/reinforcement-learning/1977-werbos.pdf>.

- [34] K. Shibata Dynamic Reinforcement Learning for Actors *arXiv preprint*, 2025, doi: 10.48550/arXiv.2502.10200.
- [35] B. Sun and E. van Kampen Incremental Model-Based Global Dual Heuristic Programming with Explicit Analytical Calculations Applied to Flight Control *Engineering Applications of Artificial Intelligence*, vol. 89, pp. 103425, 2020, doi: 10.1016/j.engappai.2019.103425.